ISSN 0236-2457

ASTRONOMICHESKII TSIRKULYAR

Published by the Eurasian Astronomical Society
and Sternberg Astronomical Institute

No. 1614, 2014 October 22

ACTIVE PROCESSES ON THE SUN AND THEIR GEOEFFECTIVENESS[1]

G.A. Porfir'eva and G.V. Yakunina

Moscow State University, Sternberg Astronomical Institute
13 Universitetskij prospekt, Moscow, 119234 Russia
E-mail: yakunina@sai.msu.ru

Received September 3, 2014

Abstract. Results of observations during last decades are revised to analyze relations between properties of flares and Coronal Mass Ejections (CMEs) accompanied by geomagnetic storms. The mass, width and velocity of CME is statistically related with flare flux. Solar Proton Events (SPEs) happen often in super active regions (SARs) with $\beta\gamma\delta$ magnetic configuration. Variations of direction and velocity of a CME, propagating through the heliosphere, influence on its geoeffectiveness are reviewed. Some aspects of the influence of the flares on the properties of the Earth's ionosphere are considered.

Heliospheric and geomagnetic disturbances are believed to be mainly caused by solar Coronal Mass Ejections. CMEs origins are due to magnetic reconnection in the low corona and accompanied by global reconstruction of magnetic field and can occur in association with solar flares, filament eruptions and streamer ejections. Temporally and spatially related CME and flare, arising from a common AR is considered to be an associated CME/flare. Solar plasma ejections have a great influence on the space weather and can cause strong magnetic storms on the Earth. The strength of the storm depends on many factors, and simple one-to one relation between the flare strength and its geoeffectiveness is not observed but there exist statistical relations between properties of CMEs and associated ARs. The more massive, quick and wide CMEs are statistically associated with the more energetic flares. The greater area of the AR is the stronger flares and geomagnetic storms are. The variation of the CMEs parameters during their propagation in the corona can significantly influence the CMEs geoeffectiveness.

Detailed analysis of data of observations obtained during 1996–2006 was fulfilled by Aarnio et al. (Aarnio A.N., Stassun K.G., Hughes W.J., McGregor S.L., Solar Phys. **268**, 195, 2011). They used the NASA CME catalog based on white-light observations with the LASCO (Large Angle Spectroscopic Coronograph) aboard SOHO (Solar and Heliospheric Observatory) and GOES (Geostationary Operational Environmental Satellite) flare database. In this period 13,862 identified CMEs and 22,674 flares were registered, among which there were 6733 CMEs with measured mass, width and velocity and 12,050 flares with known heliographic coordinates. Using the criteria for CME-flare temporal separation ($10^m - 80^m$) and position angular difference ($\pm 45°$), 826 associated CME/flare pairs were chosen.

[1]Talk presented at the Interdisciplinatory Colloquium on Cosmic Factors of Evolution of the Biosphere and Geosphere, Moscow, May 21–23, 2014.

Table 1:

Flare class	CME width
B	$42^\circ \pm 4^\circ$
C	$53^\circ \pm 0.9^\circ$
M	$63^\circ \pm 0.8^\circ$
X	$80^\circ \pm 10^\circ$

Statistically CME mass increases with flare flux: $\log M_{\rm CME} = (18.5 \pm 0.27) \times 0.70 \log F_{\rm fl}$. Here the mass of a CME $M_{\rm CME}$ is in grams and the flare flux $F_{\rm fl}$ is in W m^{-2}.

CMEs accompanied by flares have higher average velocities ($V_{\rm av} = 495 \pm 8$ km s^{-1}) than the CMEs not associated with flares ($V_{\rm av} = 422 \pm 3$ km s^{-1}). The relation between CME velocity and flare flux is presented in Fig. 1 composed by us using the data from (Kumar P., Manoharan P.K., Uddin W., ApJ, **710**, 1195, 2010; Moon Y.-J., Choe G.S., Wang H., Pak Y.D., Cheng C.Z., J. Korean Astron. Soc. **36**, 61, 2003; Porfir'eva G.A., Yakunina G.V., Oreshina A.V., Proc. Conf. Solar and Solar-Earth Physics, 2010, St.Petersburg, 331, 2010; Zhang J., Dere K.P., Howard R.A., Vourlidas A., ApJ, **604**, 420, 2004; Zhang J., Dere K.P., Howard R.A., Kundu M.R., White S. M., ApJ, **559**, 452, 2001). The results by Arnio et al. (2011) agree well with the results presented in (Andrews M. D., Solar Phys, **218**, 261, 2003; Kuznetsov V.D., Plasma heliophysics, IKI RAN, Moscow, 1, 82 (Russian), 2008; Yashiro S., Michalek G., Akiyama S., Gopalswamy N., Howard R.A., ApJ, **673**, 1174, 2008).

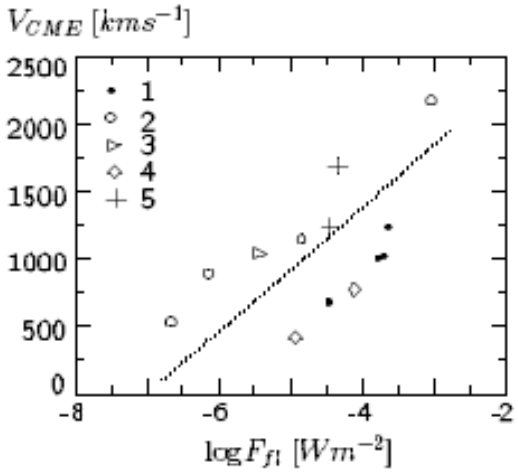

Figure 1: Relation between observed velocities V in km s^{-1} and fluxes of associated flares F in W cm^{-2}: (1) four CMEs on 1997.11.24–25 AR NOAA 9286; (2) four CMEs on 1997.05.16, 1997.02.23, 1998.06.11 and 1997.11.06 in the order of increasing velocities V; (3) CME on 2000.10.25; (4) two CMEs on 2003.11.20 AR NOAA 10501; (5) two CMEs on 2003.10.18 AR NOAA 10484.

Proton flux is believed to play an important role in producing geomagnetic storms. Strong proton events often occur in ARs being large δ-islands, when umbrae of opposite magnetic polarities are immersed in a common penumbra or having a $\beta\gamma\delta$ magnetic configuration. Such ARs are superactive (SARs) (Künzel S.W., Astron. Nachr., **285**, 271, 1960; Warwick

C., ApJ, **145**, 215, 1966; Porfir'eva G.A., Yakunina G.V., Delone A.B., IJGA, 6, No. 2, GI 2003 10.1029/2004GI000093 20 January 2006). Tian L., Liu Y., Wang J., (Solar Phys., **209**, 361, 2002) considered 29 SARs existing during 22 and 23 solar cycles. Some parameters were used to describe their activity: XRI is the X-ray flare index evaluating the sum of the flares, multiplied on their importance, the largest area $S\,\mu$h, 10.7-cm peak flux, proton flux F_p and geomagnetic index A_p. A storm begins if $A_p > 29$. Storms with $50 < A_p < 100$ are considered as strong ones. We present the results given in Tables 1 and 2 of Tian et al. (2002) as diagrams in Fig. 2 where the values for large ARs ($S > 1000\,\mu$h) and middle ARs ($S < 1000\,\mu$h) are presented, see also Figs. 2–4 in (Porfir'eva G.A., Yakunina G.V., Delone A.B., Izv. RAN, ser. Phys., **70**, No. 1, 80, 2006). There is no simple relation between the flare strength, proton flux and A_p index but statistically the larger the area of the AR the higher the X-ray flare index and geomagnetic index A_p. Compact ARs can cause severe storms.

The magnetic structure of an AR is described by tilt angle φ between the axis connecting the leading and following magnetic polarities in the AR and the solar equator, defining the general AR orientation, and free-force parameter α showing magnetic field nonpotentiality and delineating helicity of small-scale magnetic field. The magnetic line vortices can be explained by the action of the Coriolis force on rising expanding magnetic tubes in ARs. According to numerous investigations, for typical ARs $|\varphi| < (30°–40°)$, $|\alpha| < 0.02\times10^{-6}\,\mathrm{m}^{-1}$ (Bao S.D., Pevtsov A.A., Wang T.J., Zhang H. Q., Solar Phys., **195**, 75, 2000; Fisher G.H., Fan Y., Longcope D.W. et al., Solar Phys., **192**, 119, 2000; Linton M.G., Longcope D.W., Fisher G.H. et al., ApJ, 469, 954, 1996; Pevtsov A.A., Canfield R.C., Metcalf T.R., ApJ, **425**, L117, 1994; Tian et al., 2002; Tian L., Bao S., Zhang H., Wang H., A&A, **374**, 294, 2002, Tian et al., Zhang H., Tong H., Jing H., Solar Phys., **189**, 305, 199). ARs usually obey the Hale-Nicholson and Joy laws. Observations show that parameter α is mainly negative in the northern hemisphere and positive in the southern hemisphere independently of the solar cycle. By their properties SARs stand out among other ARs. They have larger areas S, produce stronger flares, more energetic proton fluxes and CMEs. Their tilt angles $|\varphi| > (30° - 40°)$ and parameter $|\alpha| < 0.02 \times 10^{-6}$ m^{-1}, as we can see, for example, from the diagrams shown in Fig. 1 (Porfir'eva G.A., Yakunina G.V., Delone A.B., Proc. IAU Sympos. No. 223, 295, 2004).

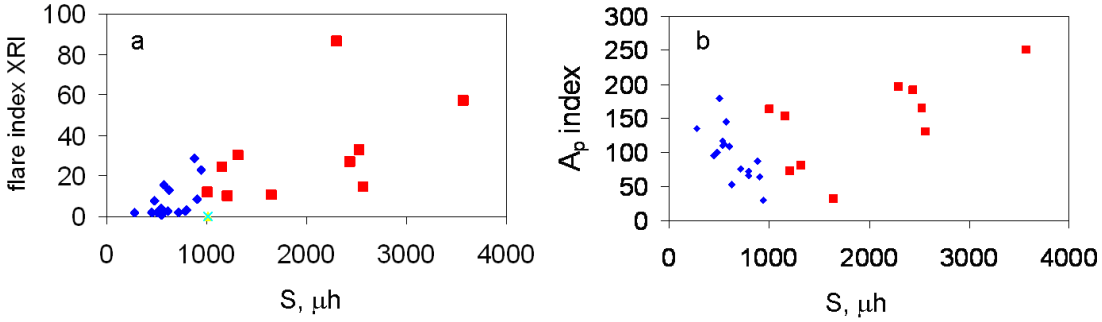

Figure 2: Relation between the X-ray flare index XRI and spot area S (a) and between geomagnetic index A_p and spot area S (b) for large (■) and middle (♦) SARs.

The magnetic helicity characterized by parameter α is known to be changeable inside the AR area. The flare activity is related to magnetic helicity and its changes. Statistically

preflare helicity of the ARs producing strong flares not accompanied by CMEs is smaller than helicity of the ARs producing flare-associated CMEs, as it was shown by Nindos A. and Andrews M.D. (ApJ, **616**, L175, 2004), who analyzed 133 events that occurred during 1966–1999, of which 78 events were associated with big flares. They found that $\alpha = 0.018 \pm 0.010$ Mm^{-1} for the ARs with flares not accompanied by CMEs and $\alpha = 0.035 \pm 0.018$ Mm^{-1} for the ARs in which CME-associated flares were observed.

Observations aboard LASCO SOHO give information in the nearest heliosphere up to distances of 20–30 $R_\odot$. Variations of velocity and direction of propagation of a CME play an important role for whether and when the CME will reach the Earth. At the solar minimum slow CMEs have difficulties to overcome straining forces of the overlying magnetic field, obeying the polar magnetic field of the Sun and tending to propagate from regions with high magnetic-energy density to sites of lower magnetic-energy density near the heliographic current layer. Analogously, inhomogeneities in the longitudinal magnetic field strength might cause a deflection of a CME in the azimuthal direction east- or westward depending on the particular magnetic-field structure, as discussed by Shen C.,Wang Y., Gui B., Ye P., Wang S. (Solar Phys., **269**, 389, 2011). At an early stage a CME may deflect by 20–30° from high latitudes toward the solar equator, as for the case of the slow, gradually accelerated CME on 8 October 2007 (Shen et al., 2011; Wang Y., Zhang J., Shen C., J. Geophys. Res., **114** (A13), 10104, 2009). Propagating in the field of view (FOV) of the COR1 STEREO B the CME was continuously deflecting toward the ecliptic plane from position angle PA$\sim$ 306° to PA$\sim$ 276° and beyond 5.5 $R_\odot$ in the COR2 FOV it was propagating almost radially. The difference images of the CME for three time instants are presented in Fig. 3, where **a** is for 11:51–11:21 UT, **b** for 13:11–12:41 UT, and **c** for 14:31–14:01 UT (the radial direction is shown with yellow, CME angular width with red and direction of the shock wave with blue lines). The CME was seen along its axis, and the observed images were cross sections of a helical rope. A similar slow deflected CME of 8 November 2008 was studied by Kilpua E.K.J., Pomoel J., Vourlidas A. et al. (Ann. Geophys., **27**, 4491, 2009).

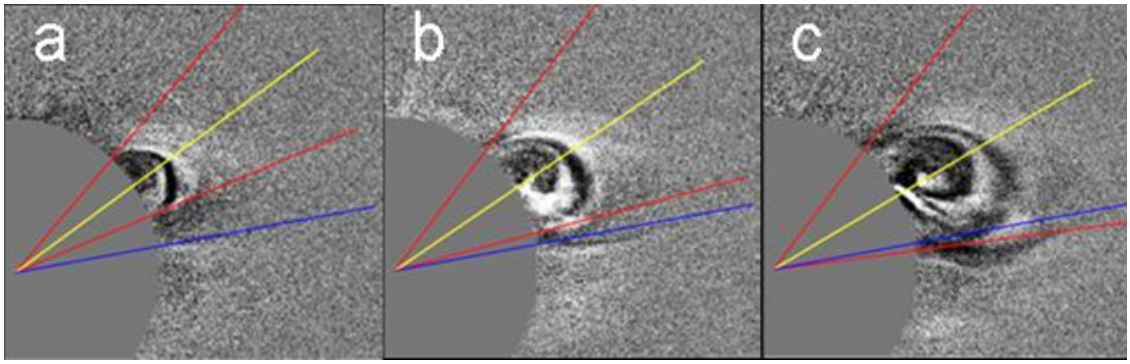

Figure 3: Deflected slow CME on 2007 October 8 by COR1 STEREO B, based on Fig. 1 from Shen et al. (2011).

Earlier the CMEs deflection in the meridian plane was investigated on the basis of Skylab observations of 1972 and 1974 (MacQueen R.M., Hundhausen A.J., Conover C.W., J. Geophys. Res., **91**, 31, 1986). An average deflection toward the ecliptic plane of $\sim 2.2°$ was found. In (Cremades H., Bothmer V., Tripathi D., Adv. Space Res., **38**, 461, 2006; Cremades H., Bothmer V., A&A, **422**, 307, 2004) 124 structured flux-rope CMEs with

known information on the associated source regions (SRs) were analyzed. The observations with LASCO, EIT, MDI SOHO and ground-based Hα images during 1996–2002 were used. The SR is the active region, where the CME originated. The PA of an AR (or a flare) was calculated from its heliographic coordinates. Spatial and temporal coincidence between the CME and its SR was required. Comparing positions angles (PAs) of the CMEs and SRs, the authors found that during 1996–1998 (near the minimum) central PAs of the structured CMEs deflected for about 20° to lower latitudes, toward the solar equator. At times of the high activity (1999–2002) the deviations ranging from several degrees to 20–40° fluctuated towards the solar poles or equator without a systematic trend, see Fig. 19 in (Cremades et al., 2004). Yashiro et al. (2008) investigated the spatial relation between associated flares and CMEs comparing their PAs. For the 1996–2005 LASCO SOHO observations they found 496 flare-CME pairs considering limb events. They concluded that differences between flare PAs and CME central PAs were $\sim 17°$.

Simultaneous white-light observations in from different viewpoints in space carried out with the wide-angle imagers HI-1 and HI-2 aboard STEREO A and B give a possibility to follow a CME almost to the Earth and to derive the CME shape and direction of its propagation through the heliosphere. Deflection in longitudinal direction was analyzed in (Lugaz N., Hernandas-Charpak J.N., Roussev I. I., Davis C.J., Vourlidas A., Davies C.J., ApJ, **715**, 493, 2010; Liu Y., Davis J. A., Luhmann J.G., Vourlidas A., Bale S.D., Lin. R. P., ApJ, **710**, L82, 2010, a.o.). The observations have shown that CMEs (or their pieces) might deflect monotonically or with some temporal fluctuations toward the east (in some cases) or toward the west (in other cases) by about 5–30° up to the heliocentric distances of 100–150 $R_\odot$. The CME of 2008 April 26 propagated eastward from the Sun–Earth direction, and its deflection increased by more than 25° when the CME was moving away from the distance of 20 $R_\odot$ ($\Phi = -11°$) to the distance of 130 $R_\odot$ ($\Phi = -37°$). The result agrees well with $\Phi = -11°$ of Thernisien et al. (Ternisien A., Vourlidas A., Howard R., Solar Phys., **256**, 111, 2009) and $\Phi = -28°$ by Wood et al. (Wood B.E., Howard R.A., ApJ, **702**, 901, 2009). The CME velocity was determined to be 534 km s^{-1} and the arrival time to STEREO B was predicted by Lugaz et al. (2010) with an error of $\sim 11^h$.

Wood et al. (2009) modeled the appearance of the CME on 2008 May 17 by a combination of two expanding fronts F1 and F2. The CME was very fast for the solar minimum and its velocity reached ∼1120 km s^{-1}. A slice through the ecliptic plane of the 3D CME model is presented in Fig. 4a. The locations of the Sun and STEREO A and B on the heliocentric coordinates XY are shown. The front F1 was oriented $\sim 2°$ south from the ecliptic and $\sim 52°$ to the east and the front F2 was $\sim 8°$ north and $\sim 26°$ to the east from the Sun–Earth direction. Their ecliptic coordinates, longitude l and latitude b, were $l = 188°$, $b = -2°$ for F1 and $l = 213°$, $b = 8°$ for F2. The results agree well with the trajectory defined by Thernisien et al. (2009), who used flux rope fitting (Ternisien A.F.R., Howard R.A., Vourlidas A., ApJ, **652**, 763, 2006). The F2 moved almost radially toward STEREO B, corresponding to the position angle of the B1.7 flare at the center of the solar disc, and the F1 deflected by $\sim 26°$ as compared to the direction of the F2 moving away from both STEREO A and STEREO B. The STEREO A and corresponding 3D reconstructed image are shown in Fig. 4b, c (by Fig. 1 from Wood B.E., Howard R.A., Thernisien A., Plunkett S.P., Socker D.G., Solar Phys., **259**, 163, 2009).

Solar flares accompanied by proton fluxes affect the structure of the D region in the Earth's ionosphere. The conditions in the D region located in the undisturbed state at the

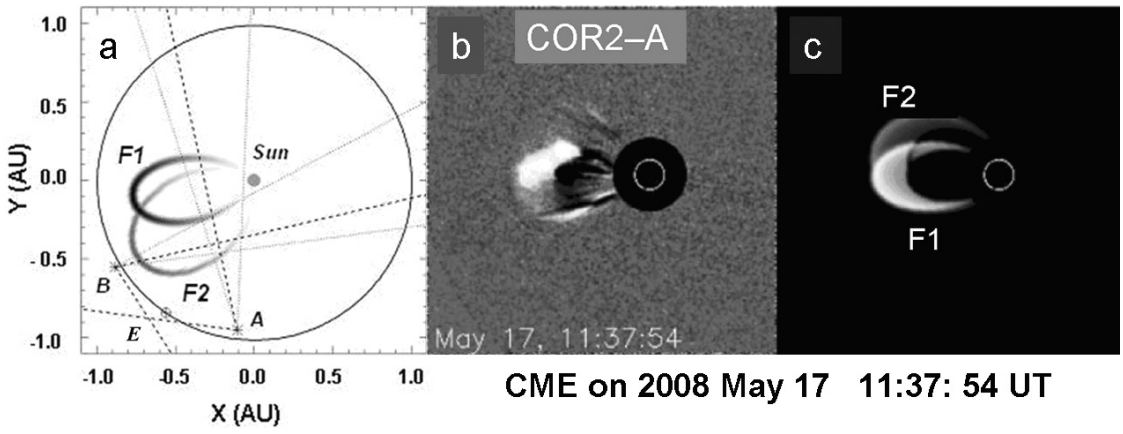

Figure 4: CME on 2008 May 17–18: the location of the fronts F1 and F2, FOVs of the HI1 and HI2 are shown (a); STEREO COR2-A (b) and synthetic (c) images, by Fig. 1 and Fig. 3 from Wood, Howard, Thernisien et al. (2009).

heights from 50 to 90 km are important for the propagation of radiowaves. Between the lower D region and the oceans (and ground) an Earth–ionosphere waveguide is formed in which the mean frequencies (3–30 kHz) propagate usually without interference, going round the Earth's globe and causing Schuman resonance (SR) phenomenon. Undergoing multiple reflections between the Earth surface and the lower boundary of the ionosphere D region, SR waves give rise to a set of resonance lines. Properties of the D region influence on the intensity, amplitude and phase of radiowaves. Energetic particles can produce additional ionization in the lower D region and perturb its upper boundary. Changes in the D region are characterized by two parameters: reflection height H' and sharpness factor β, which is a measure of the rate of the electron density variation with height in km^{-1}.

Singh B., Tyagi R., Hobara Y., Hayakawa M. (J. Atmosph. Solar-Terr. Phys., **113**, 1, 2014) analyzed the influence of the flares with the SEP on the structure of the D region. On the low latitude station near Agra ($\varphi = 14°55'$, India) the 19.8-kHz emission from the NWC transmitter in Australia was recorded during the X1.4/2N flare on 2011 September 22 (NOAA 11302, N11E74, flare peak at 10:29–11:01 UT, start of the SPE on September 23 at 02:00 UT, maximum at 22:25 UT, duration $\sim 36^h$) and the X1.1 flare on 2012 July 6 (NOAA 11515, S18W50, flare peak at 23:01–23:08 UT, start of the SPE on July 7 at 00:00 UT, maximum at 07:45 UT, duration 10^h). The event of 2011 September 22 is presented in Fig. 5.

We can see that the proton SR frequency increased by 8.4% during the flare and later decreases to 4.35% when the proton flux peaked. Similar changes occurred during the flare and following proton flux on 2012 July 6–7. The results can be interpreted by the model accounting for the growth of ionization in the upper part of D region due to the X-ray flare burst and high ionization in the lower D region (at 50–60 km) in the polar region during the SPE. In (Singh As. K., Singh A. K., Singh R., Singh R.P., Astrophys. Space Sci. **350**, 1, 2014) 32 flares happened during 2011–2012 are analyzed using the record of the 19.8-kHz emission from Australia. Analyzing the changes in the signal amplitude, the values of H' and β corresponding to flares of different importance were defined. If, for the quiet ionosphere above the equator of the Earth, $H' \sim 71$ km and $\beta \sim 0.43$ km^{-1}, during flares

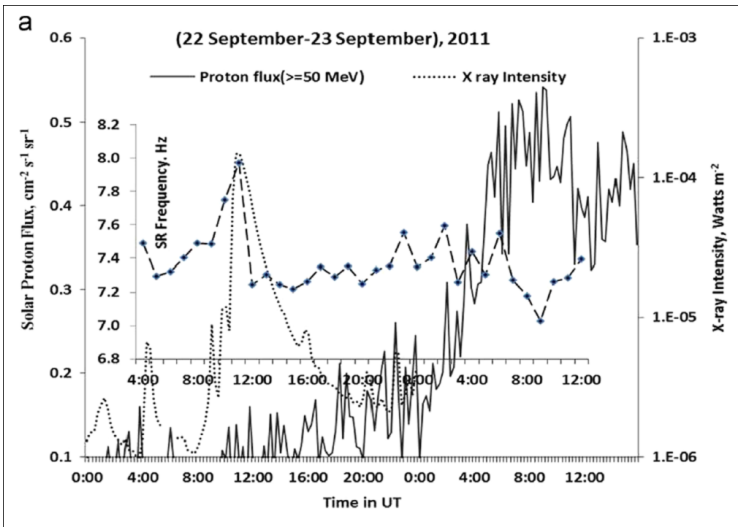

Figure 5: Relations between the X-ray intensity of the X1 flare on 2011 September 22, proton flux and changes in the SR frequency, by Fig. 3a from Singh B. et al. (2014).

$65 < H' < 70.6$ km and $0.433 < \beta < 0.470$ km s^{-1} depending on the flare importance. Electron density N_e in the D region can increase several times. Thus, during the M5 flare of 2012 August 18 N_e increased in the ionosphere above the Earth's equator by 320%.

Summary

Results of the observations of flares and active processes accompanied by geomagnetic disturbances during the last decades are considered. Some statistical relations between the properties of the flares, CMEs and magnetic disturbance characteristics are discussed. The stronger the flare, the greater the mass of the associated CME. The widths of flare-associated CMEs are statistically proportional to the flare flux and are $80°\pm10°$, $63°\pm1.8°$ and $42°\pm1.4°$ for X, M and B class flares. Flare-associated CMEs reach higher velocities than unassociated ones. Their averaged velocities are 495 ± 8 km s^{-1} and 422 ± 3 km s^{-1}, respectively. Energetic proton events occur often in ARs with a δ or $\beta\gamma\delta$ magnetic configuration. For such ARs the larger the area, the higher flare index and the greater geomagnetic index A_p. The problem of CME propagation through the heliosphere is discussed. Changes in the velocity and direction are important, they determine whether and when the CME reaches the Earth. The influence of flares and SPEs on the properties of the D region of the ionosphere is considered. During the flares the reflecting region height (above the surface of the Earth) decreases and N_e inside it increases.

Активные процессы на Солнце и их геоэффективность

Г.А. Порфирьева и Г.В. Якунина

Московский Государственный университет имени М.В. Ломоносова
Государственный астрономический институт имени П.К. Штернберга
Россия 119234 Москва, Университетский проспект 13
E-mail: yakunina@sai.msu.ru

Резюме. Рассмотрены результаты наблюдений последних десятилетий с целью проанализировать связи между свойствами вспышек и корональных выбросов массы (КВМ), сопровождаемых геомагнитными бурями. Масса, ширина и скорость КВМ статистически связаны потоком вспышки. Солнечные протонные события часто происходят в сверхактивных областях с магнитной конфигурацией типа $\beta\gamma\delta$. Исследованы вариации направления и скорости КВМ, распространяющегося в гелиосфере, и его геоэффективность. Рассмотрены некоторые аспекты влияния вспышек на свойства ионосферы Земли.